Ceramics International **23** (1997) 389–399

PII: S0272-8842(96)00041-7
0272-8842/97/$17.00+.00

Final Stages of Sintering of Ceramic Materials: Effect of Residual Porosity and Microstructure on Mechanical Characteristics of Surface

A. L. Yurkov,*[a] T. A. Sarkisyan,[a] D. A. Ivanov[b] & R. C. Bradt[c]

[a]Department of Ceramics, Mendeleev University of Chemical Technology of Russia, Moscow 125190, Russia
[b]Moscow University for Aviation Technology, Moscow, Russia
[c]Metallurgical and Materials Engineering Department, University of Alabama, Tooscaloosa, AL 35487-0202, USA

(Received 20 July 1995; accepted 30 January 1996)

Abstract: The final stage of sintering determines the mechanical characteristics of material. Usually the final stages of sintering are optimized via residual porosity and grain size and shape (that are believed to control mechanical characteristics) with the help of temperature and time of sintering.

Elimination of residual porosity at final stage of sintering may be accompanied by excessive grain growth. Grain growth may take place as a result of secondary recrystallisation during solid state sintering. During sintering in the presence of a liquid phase, grain growth may be a result of "dissolution–precipitation" mechanism, as well as a result of direct coalescence owing to migration of solid solid boundaries.

A study of the load dependence of hardness and deviations of values of microhardness from the average value can be an instrument of optimization of the final stages of sintering. © 1997 Elsevier Science Limited and Techna S.r.l.

1 INTRODUCTION

During the initial stages of sintering, grain boundaries of particles of sintered compact develop at the small cross-sections of the contact regions and pores are continuous. At the intermediate stage of sintering, pores form a continuous network, attached to grain boundaries. Then the system of continuous pores breaks down and more or less equilibrium-shaped isolated pores form at the grain boundaries.[1]

The pores at grain boundaries or grain edges or corners limit final densification, since volume diffusion is usually much slower than grain boundary diffusion. The final stage of sintering determines microstructure details and the remaining porosity.

Elimination of residual porosity at the final stage of sintering may be accompanied by excessive grain growth. Grain growth may take place as a result of secondary recrystallisation during solid state sintering. During sintering in the presence of liquid phase, grain growth may be a result of a "dissolution–precipitation" mechanism, as well as a result of direct coalescence owing to migration of solid–solid boundaries.

Grain boundary stresses are important in determining many properties of polycrystalline ceramics.[2] Although the stresses are independent of grain size, spontaneous cracking usually occurs predominantly in large grain sized samples, because the reduction of internal strain energy is proportional to the cube of particle size, whereas the increased surface energy caused by the fracture is proportional to the square of the particle size. Mechanical properties of many ceramic systems are maximized with high density and small grain

Now at: 5164 CMMG, 5047 Gullen Mall, Detroit, MI 48202, USA.

size. However, these characteristics are sometimes in contradiction.

Mechanical properties of the surface (load dependence of hardness, coefficient of variation of values of hardness, Meyer's index) are very sensitive characteristics in the development of the structure of polycrystalline materials.[3]

The aim of this article is to investigate different variants in the development of the homogeneous and inhomogeneous structure of ceramics at the final stage of sintering by traditional means (residual porosity, grain size distribution, etc.) and their correlations with the mechanical characteristics of the surfaces of such ceramics. Silicon nitride, SiAlON, aluminium nitride and aluminium oxide ceramics were analysed.

2 EXPERIMENTAL PROCEDURE

2.1 Preparation of samples

2.1.1 Silicon nitride and SiAlON based materials

The investigated materials were silicon nitride based materials (N1, N2) and SiAlON based materials of the system Y–Si–Al–O–N (N3) (Table 1). Composition, preparation and characteristics of sample N3 are described in Ref. 3 where it is called N2.

All samples were prepared from silicon nitride powder, having specific surface area of 25–30 m^2/g. (N > 37.0%, free Si < 1.0%, O < 2.0%, Al < 0.2%, Fe < 0.1%, Ca < 0.01%). The powder was prepared by plasmochemical synthesis. The additions were prepared by plasmochemical synthesis; oxides and AlN had specific surface area of 15–18 m^2/g.

The powders were mixed in a planetary mill in Teflon drums in acetone. After mixing the powders were dried, disintegrated and cold isostatically pressed without binders at a pressure of 1000 MPa.

The sample N1 was sintered at $T = 1800°C$, $P = 1.5$ MPa for 1 h. The samples N2 and N3 were sintered according to a two-step regime. During the first cycle the samples were sintered at a temperature of 1800°C and a pressure of 1.5 MPa for 15 min. up to zero accessible porosity. During the second cycle the pressure was raised up to 70 MPa and held at 1750°C for 1 h (Table 1). All the sintered materials are dense (porosity < 1–2% – Table 2). The structure of all the specimens consists of fine grains. The grains are isometric or short-prismatic ($d = 1$–2 mm, $l/d = 2$). The glassy phase is in the form of continuous and discontinuous layers between the grains and has a refractive index of 1.6.

2.1.2 Aluminium nitride materials

The aluminium nitride powders are prepared by carbothermal synthesis (Table 3). The average grain size is 0.6–0.8 μm. The sample N1 was fabricated from powder N2, the samples N2 and N3 were prepared from powder N1.

Yttrium oxide additive (2 wt%) was introduced in green mixtures of sample N1 during dry milling. In the powder of samples N2 and N3 the additive $Ca(NO_3)_2 \cdot 4H_2O$ was introduced in the form of a solution of salt in acetone (in the amount of 2.5 wt% CaO). The binder for pressing was raw rubber, dissolved in benzene (1.5% in dry condition). The samples were pressed in steel dies at a pressure of 200 MPa.

The sintering regime was conducted in an inert–partly reducing atmosphere (N_2–N_2/H_2) in graphite containers at a temperature of 1850°C for sample N1, and at a temperature of 1850°C for samples N2 and N3. The sintering time was 2 h.

2.1.3 Aluminium oxide materials

The starting powder for aluminium oxide materials was α-Al_2O_3 (average grain size 0.8–2 μm) with addition of 0.5 wt% MgO, that was introduced during milling in the form of salt of magnesium.

Material N1 was sintered from starting powder with additives of Cr_2O_3 and SiO_2 (total amount 10 wt%) during 2 h at a temperature of 1600°C. Material N2 was hot pressed in graphite dies during 0.5 h at a temperature of 1600°C (N1) and 1750°C (N2).

2.2 Characterisation and testing of materials

The materials were characterised by petrographical analysis, scanning electron microscopy (SEM),

Table 1. Starting powders and compositions of sintered silicon nitride and SiAlON based materials

NN	Specific surface area (m^2/g) Si_3N_4	Additions	Addition	Method of manufacturing	Main phase	Additional phase
1	18	15–18	Y_2O_3–La_2O_3	sintering 1.5 MPa N_2	β-Si_3N_4	glassy phase
2	18	15–18	Y_2O_3	sintering 1.5 MPa N_2 +HIP	β-Si_3N_4	glassy phase
3	18	15–18	Y_2O_3–Al_2O_3–AlN	sintering 1.5 MPa N_2 +HIP	β′-SiAlON	glassy phase, 12H

Table 2. Characteristics of sintered silicon nitride and SiAlON based materials

NN	Density, (g/cm^3)	Bending strength (MPa)	K_{1c} ($MPa \cdot m^{1/2}$)	HV (98.1 N) (GPa)
1	3.3	400±40	4.4±1.5	13.5±1
2	3.4	500±40	3.66±1.3	12±1
3	3.22	450±50	5.33±1.4	18±1

Table 3. Chemical composition of starting AlN powders (wt%)

NN	O	C	N	Fe	Mn	Ti	Cr	Si	B	Mg
1	0.2	0.5	33.5	0.02	0.04	0.008	0.003	0.004	0.03	0.001
2	0.2	0.5	33.5	0.001	0.001	0.001	0.001	0.004	0.01	0.001

mercury absorbtion porometry, microprobe X-ray spectral analysis and X-ray direction analysis (XDA).

The samples were diamond cut and polished. The bending strength of the samples (3-point bending) was measured, using 4×4×35 mm bars. The fracture toughness was measured by the indentation technique using the equation of Antis *et al.*[4]

Contact microhardness tester MTI-3m (design of Institute for Machine Science, Moscow) registers the depth of penetration of the indenter during increasing load, constant load and decreasing load.

The standard deviation of depth of penetration of the Vickers diamond indenter was 0.02 μm (taking into account time-depending floating of electric current of the sensor during intrusion of the indenter) and of measuring of the load was 1.5%. The speed of intrusion of the indenter into the material was about 0.3 mms $^{-1}$. The description of the contact microhardness tester MTI-3m and the principles of interpretation of indentation data are explained earlier.[35]

The value of unrelaxed microhardness HV is calculated as:

$$HV = 0.03784 * P/h^2 \tag{1}$$

where P is load (N) and h is the unrelaxed depth of penetration (μm).

The plot "load–depth of penetration" (Fig. 1) is easily converted to a plot of "microhardness–load" (Fig. 2). The plot "load–depth of penetration" may also be converted to the logarithmic plot "log P–log h".

The indentation cycle was repeated at 10 points in each specimen with a step of 0.5 mm from one point of indentation to another. The deviation of values of microhardness of materials is characterised with the help of a coefficient of variation (Fig. 3):

$$c = D/m \tag{2}$$

where D is the variance of values of microhardness from 10 points at fixed load and m is the average value.

3 RESULTS AND DISCUSSION

3.1 Indentation size effect (ISE)

The load dependence of diagonal size of indent (Fig. 4) can be modelled by the power law:

$$P = KD^n \tag{3}$$

where P is a load, K is constant and D is the length of the diagonal of the indent. The eqn (3) can be rewritten in the form:

$$P = ah^n \tag{4}$$

where a is the transformed constant and h is the depth of penetration of the indenter.

Both eqns (3) and (4) are called Meyer's law or the log-index relationship. The value of Meyer's index n is used to express a measure of ISE. If the hardness is independent of load, n must equal 2. If the hardness increases, when the applied load decreases, $n < 2$. If the hardness decreases when the applied load decreases, $n > 2$. Deviations from $n = 2$ are the measure of ISE and for a certain material in concrete specific case will be a measure of microstructural variations, surface layers, mechanochemical effects, etc.

In order to make an analysis eqn (4) may be written as:

$$\log P = \log a + n \log h \tag{5}$$

Thus, corresponding values of log P and log h can be plotted and from the slope of a straight line, Meyer's index n can be found.

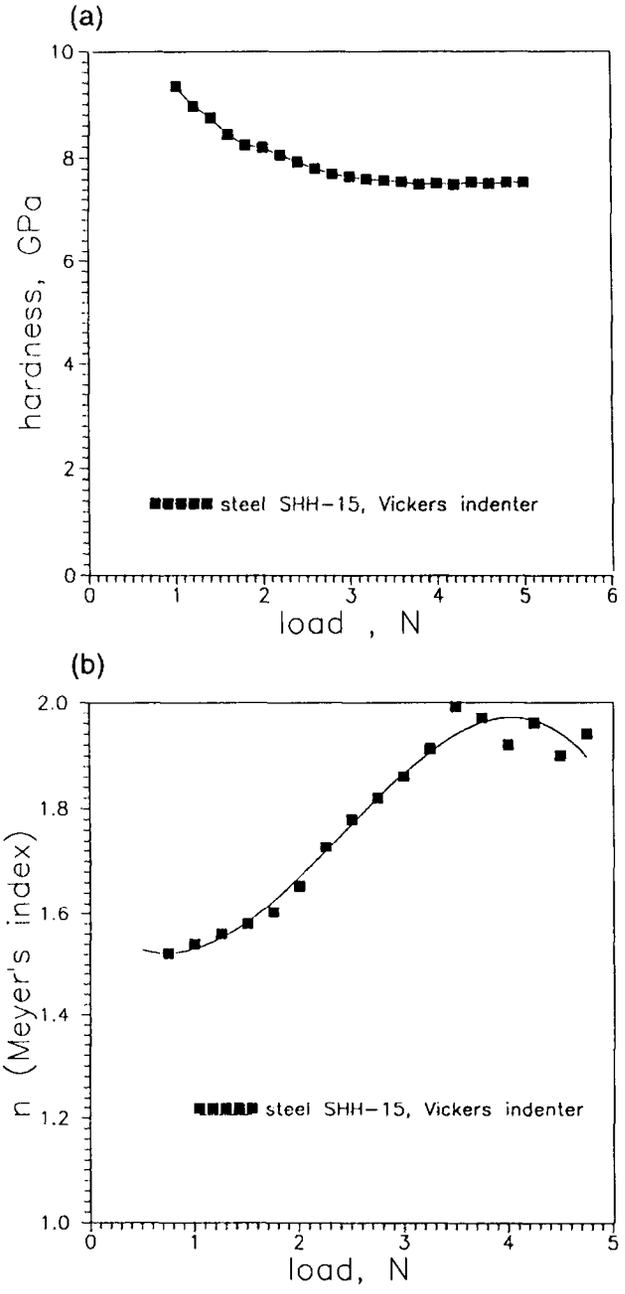

Fig. 1. Plots of (a) "hardness–load" and (b) "Meyer's index n–load". Material is steel SHH-15.

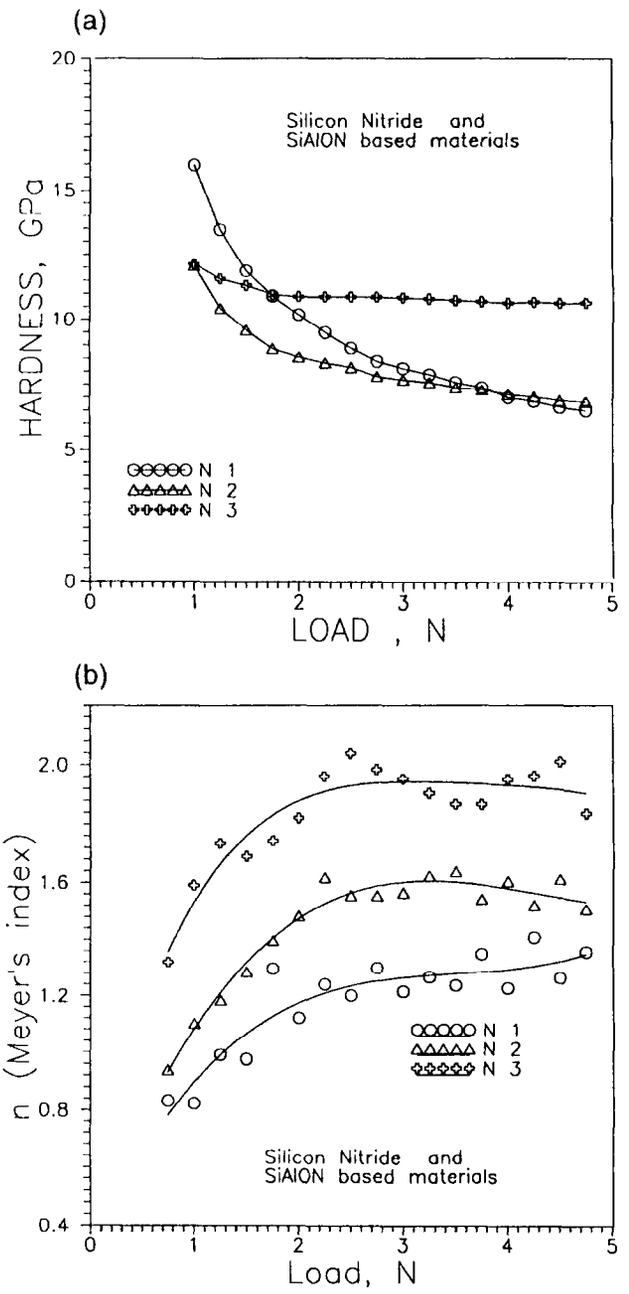

Fig. 2. Plots of (a) "hardness–load" and (b) "Meyer's index n–load" for silicon nitride and SiAlON based ceramics.

The joining of the conventional power analysis of Meyer (eqn (5)) with differentiating[3] gives the expression:

$$n = \frac{\ln(H_i/H_{i+1})}{\ln(h_i/h_{i+1})} + 2 \qquad (6)$$

Now it is possible to see (Fig. 1(b), Fig. 2(b), Fig. 5(b)) that the coefficient n is not constant. Equation (5) may be approximated as a line in a very narrow interval. The dependence of Meyer's index n vs load (depth of indentation or diagonal of indent) is shown by the differences between the mechanical characteristics of the surface layers and the inner layers of the material.[3]

Finally, in perfect materials the load dependence of hardness reaches a plateau (the border of the Indentation Size Effect),[6] as shown in Fig. 1(a) for a standard material — carbonized steel SHH-15(C: 0.95–1.1 wt%; Si: 0.15–0.35 wt%; Mn: 0.2–0.4 wt%; Cr: 1.3–1.65 wt%; S: <0.02 wt%; P: <0.027 wt%; Ni: <0.2 wt%). On the plot of "n–P" it can be seen that after a certain load (the border of ISE), Meyer's index n reaches a value of 2 (Fig. 1(b)).

In real materials there may be three variants: (1) load dependence of hardness reaches a plateau — $dH/dP = 0$, $n = 2$ (Fig. 1(a)); (2) load dependence of hardness reaches a plateau with a slope $dH/dP = \text{const}$, $n \gg 2$ (Fig. 2, sample N2); (3) load

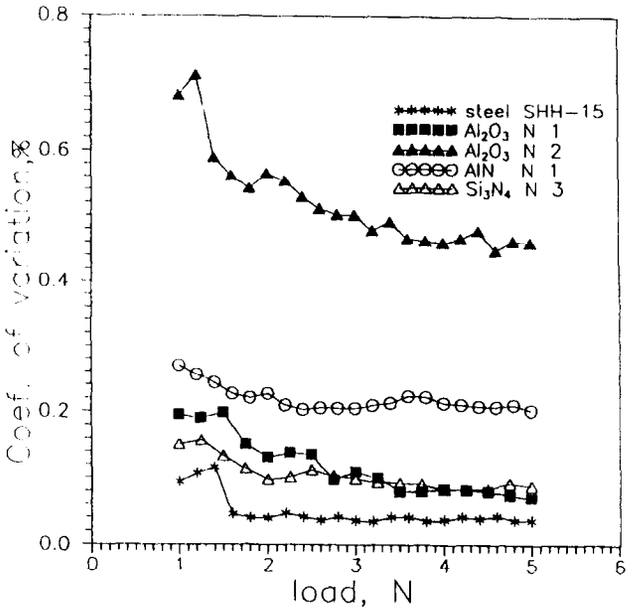

Fig. 3. Plots of "coefficient of variation–load" of steel SHH-15, SiAlON material (N3), AlN material (N3) and aluminium oxide materials (N1 and N2).

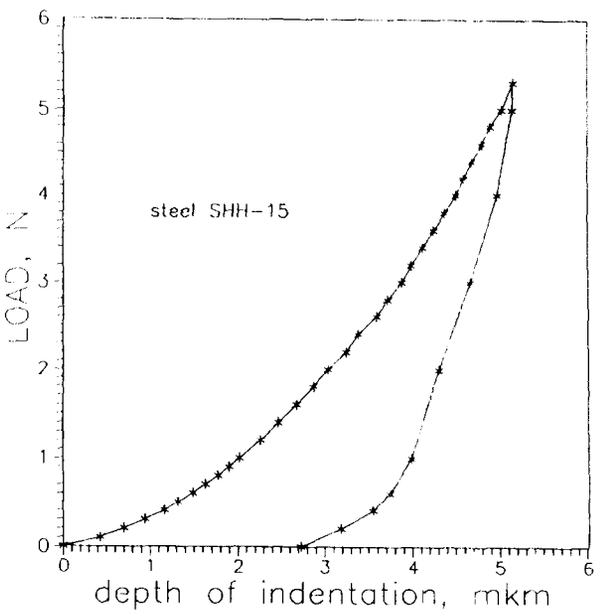

Fig. 4. Typical plot of "load–depth of indentation", registered by contact microhardness tester: upper curve is loading, lower curve is unloading. Material is steel SHH-15.

dependence of hardness does not reach a plateau, $n < 2$, $n = f(P)$ in all interval of loads (Fig. 2, sample N3). The following is an analysis of the final stages of sintering of real ceramic materials from the point of view of the mechanical characteristics of the surface (ISE, coefficient of variation).

3.2 Silicon nitride and SiAlON based materials

All the sintered materials are dense (porosity < 1–2% — Table 2). The structure of all the specimens consists of fine grains (Fig. 6).

However, there are certain differences. Silicon nitride material N1 consists of very fine grains, the grains are almost completely round in shape. Although the residual open porosity is relatively low, it is the highest among silicon nitride and SiAlON materials. We may suppose that the sintering process was determined by plastic deformation and creep, leading to a rearrangement of the particles. There are no traces of dissolution of smaller particles and growth of larger ones by materials transfer through a liquid phase, though some traces of the discontinuous layers of a glassy phase can be seen between the grains.

The mechanical characteristics are rather low (Table 2), because the sintering process is not completed. The dependence "load–hardness" would not reach a plateau: Meyer's index n diminishes with increasing load. The structure, that remains unsintered up to the end, cannot demonstrate constant resistance to the process of intrusion of the indenter.

The grains of silicon nitride material N2 are slightly elongated ($d = 1$–$2\,\mu m$, $l/d = 2$), i.e. the grains began to grow along the c-axis. The glassy phase is in the form of continuous and discontinuous layers between the grains and has a refractive index of 1.6. Compared to sample N1, there are no traces of residual porosity with dimension > 20 E. According to SEM there are traces of closed porosity in the amount of 1%. So the sintering process in sample N2 is close to its final stage.

Mechanical characteristics of sample N2 after hot isostatic pressing are almost the same as those of sample N1 after pressure sintering. However, the load dependence of hardness of sample N2 has a shallower gradient when compared to that of sample N1. This results in bigger absolute values of Meyer's index and in dependence "n–P", that tends to be flat (the case when dH/dP—const.). It also shows that the structure of sample N2 tends to final formation.

The grains of sample N3 are isometric or short-prismatic ($d = 1$–$3\,\mu m$, $l/d = 2$). The crystallographic facets of grains are strict and well-developed. The continuous and discontinuous layers of glassy phase (0.7–1 μm thick) are situated between the grains. The sintering process, including plastic deformation, rearrangement of particles and "dissolution–precipitation" through a liquid phase, has been completed. There is no open porosity. There are no traces of closed porosity. The prolongation of the sintering regime may lead only to dissolution of smaller particles and growth of larger ones by materials transfer through a liquid phase. This will

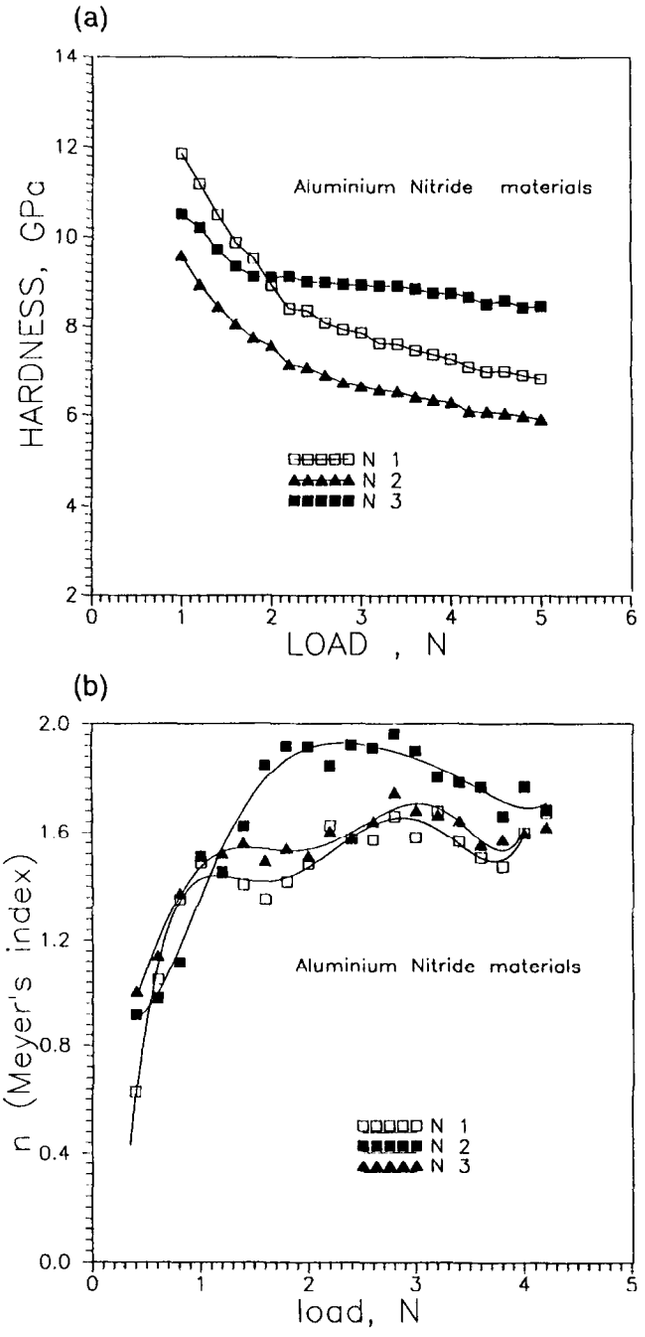

Fig. 5. Plots of (a) "hardness–load" and (b) "Meyer's index n–load" for aluminium nitride ceramics.

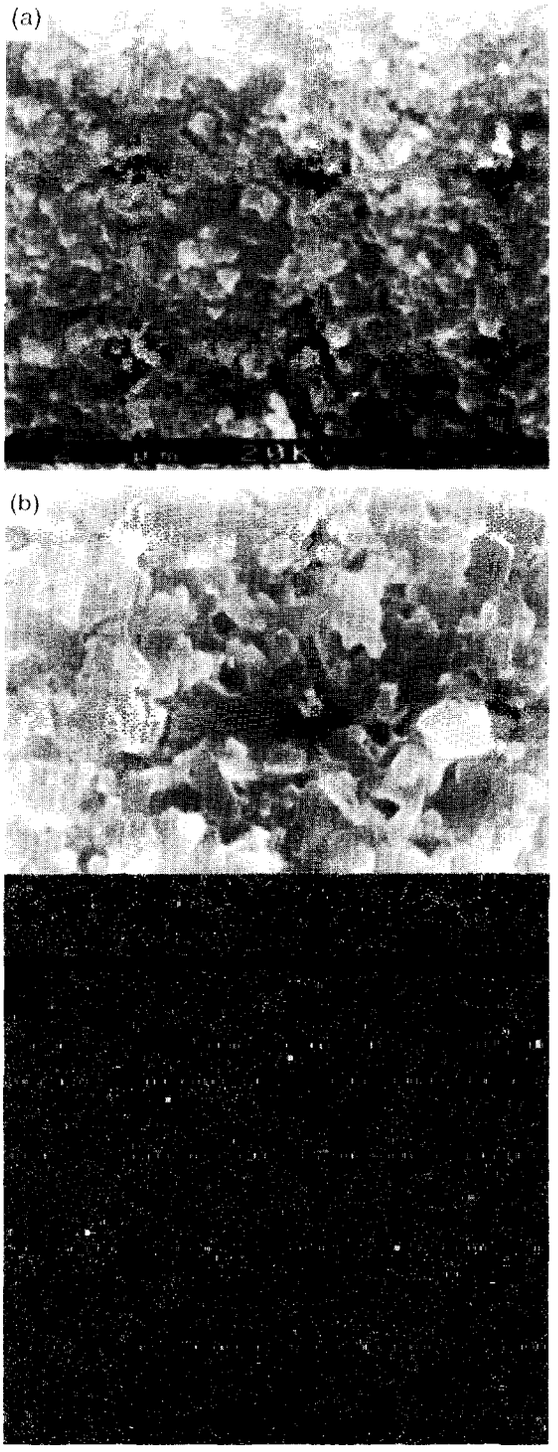

Fig. 6. Structures of silicon nitride and SiAlON based ceramics: (a) N1; (b) N2; (c) N3.

result in growth of boundary stresses and deterioration of mechanical characteristics.

The mechanical characteristics of sample N3 are slightly higher than samples N1 and N2. The "hardness–load" dependence is close to that on Fig. 1(a) for steel. Meyer's index n reaches a value of 2, that shows that $dH/dP = 0$ (within the border of ISE), and the material is capable of withstanding intrusion of the indenter, not depending upon load or depth of indentation. (The inflection on "n–P" dependence at 3 N may show the nucleation of median cracks under the indenter.)[3]

So three silicon nitride and SiAlON based materials at the final stages of sintering with different degrees of residual porosity and different average grain sizes demonstrate the different "hardness–load" dependencies (Indentation Size Effect). Dependence of the "Meyer's index n–load" makes these differences more distinctive.

3.3 Aluminium nitride materials

The sintered materials are dense. The bending strength of the materials is 280–300 MPa. Thermal

coefficient of expansion (interval 473–673 K) is 4.5×10^{-6} K. Dielectric properties at a frequency of 10^6 Hz are: tg $p\times10=5$, $\epsilon=8$.

In material 1 the distribution of grain size is very non-uniform, with the grains ranging from 3 μm to 17 μm in dimension. The form of the grains is close to isometrical, and the facets are well developed. There are two secondary phases transparent and non-transparent (Table 4). The grains of the non-transparent phase (YN, from XDA) are up to 7 μm in size and occupy sites between grains of AlN. The transparent phase (Y_2O_3) lies in the form of discontinuous layers, up to 1.5 μm thick, at the grain boundaries of AlN. The total amount of non-transparent phase (YN) is 1%, and the total amount of transparent phase is 2%. The total open porosity is about 0.5% and there are no traces of closed porosity (Fig. 7(a)–(c)).

It is possible to suppose that at the final stages of sintering, the "dissolution–precipitation" mechanism gave rise to intense grain growth. The material is almost fully dense, but the microstructure is very non-uniform. The "hardness–load" dependence did not reach a plateau (Fig. 5). Meyer's index n reaches a value of 1.6–1.7, that usually takes place when the sintering process is not finished. Here it shows that the inhomogeneous structure cannot withstand the intrusion of the indenter, not depending upon load.

The structure of material N2 is more uniform. The grain size dimension is 2–4.5 μm. The shape of the AlN grains varies from isometric to elongated short-prismatic. The refractive index of AlN differs slightly from the border of the grain to the centre (this shows an unfinished sintering process). The secondary phase is only partly crystallized, ($CaO{\cdot}6Al_2O_3$) in the form of intermediate layers 1–1.5 μm thick, and is very uniformly distributed. There is no closed porosity (SEM). The main cause of inhomogeneity is a sintering process that proceeds at different velocities in different parts of the sample.

Yet the sintering process was nearly finished, when the material became almost fully dense (open porosity 0.8%), but the grains of AlN were round in shape and had no strict crystallographic facets. So the sintering process was not truly finished the grain facets didn't appear; material N2 has the lowest values of hardness and Meyer's index did not exceed 1.6.

The structure of material N3 is close to ideal. More than 80% of the grains of AlN have dimensions of 2 mm, and the other grains do not exceed 4 μm. The refractive index of AlN is very uniform. The layers of secondary phases (< 1 μm) are uniformly distributed between the grains of AlN. The secondary phase of $CaO{\cdot}Al_2O_3$ is fully crystallized. In the place of contact between secondary phases and AlN there is no grain facet of AlN (that appear on dissolution). The grains have strict crystallographic facets and are round in shape. There are no traces of closed porosity.

Material N3 has the greatest values of hardness, and Meyer's index n nearly reaches a value of 2, showing that the sintering process resulted in a perfect structure. However, Meyer's index at low loads (near-surface layers) differs considerably from that at high loads (inner layers). It shows that differences exist in the mechanical properties of the surface layers and the inner structure.

So dense aluminium nitride materials with different structures and residual porosities demonstrate different "load–hardness" behaviour. When the material is not fully sintered (residual porosity, unformed crystallographic facets), or when the final stage of sintering provides a non-uniform microstructure, Meyer's index n is 1.5–1.7. In material free of residual porosity, with perfect structure and strict grain size distribution, Meyer's index tends to a value of 2 (Table 5).

Table 4. Data of X-ray diffraction analysis of AlN materials

Material	Main phase	Secondary phases
1	AlN	Y_2O_3, YN
2	AlN	$CaO{\cdot}Al_2O_3$
3	AlN	$CaO{\cdot}6Al_2O_3$

3.4 Aluminium oxide materials

The aluminium oxide material N1 is a conventional sintered dense alumina with a rather strict grain size distribution with dimension not exceeding 3 mm. The bending strength is 650 ± 50 MPa,

Table 5. Porosity of silicon nitride, SiAlON, aluminium nitride and aluminium oxide materials

Porosity (%)	Silicon nitride and SiAlON based			Aluminium nitride			Aluminium oxide	
	1	2	3	1	2	3	1	2
Open porosity (<20 Å)	0.60	0.19	0.00	0.16	0.16	0.05	0.02	0.16
Open porosity (<20–500 Å)	0.25	0.00	0.05	0.64	0.23	0.00	0.00	0.00
Closed porosity (SEM)	0.00	1.00	0.00	0.00	1.00	0.00	0.00	0.00
Total porosity	0.85	1.19	0.05	0.80	1.39	0.05	0.02	0.16

$K_{1C} = 5.8 \pm 0.66\,\mathrm{MPa \cdot m^{-1/2}}$ (determined by notch bend test). It was taken as an example of a material that demonstrates normal characteristics of surface, as well as good silicon nitride, SiAlON or aluminium nitride materials or others.

The "load dependence of hardness" of aluminium oxide material N1 (Fig. 8(a)) looks like such dependencies of "normally" sintered materials – – such as SiAlON N3 and aluminium nitride N2. The dependence of Meyer's index n varies around the value of 2 (the ups and downs corresponding to nucleation of cracks under the indenter).[3]

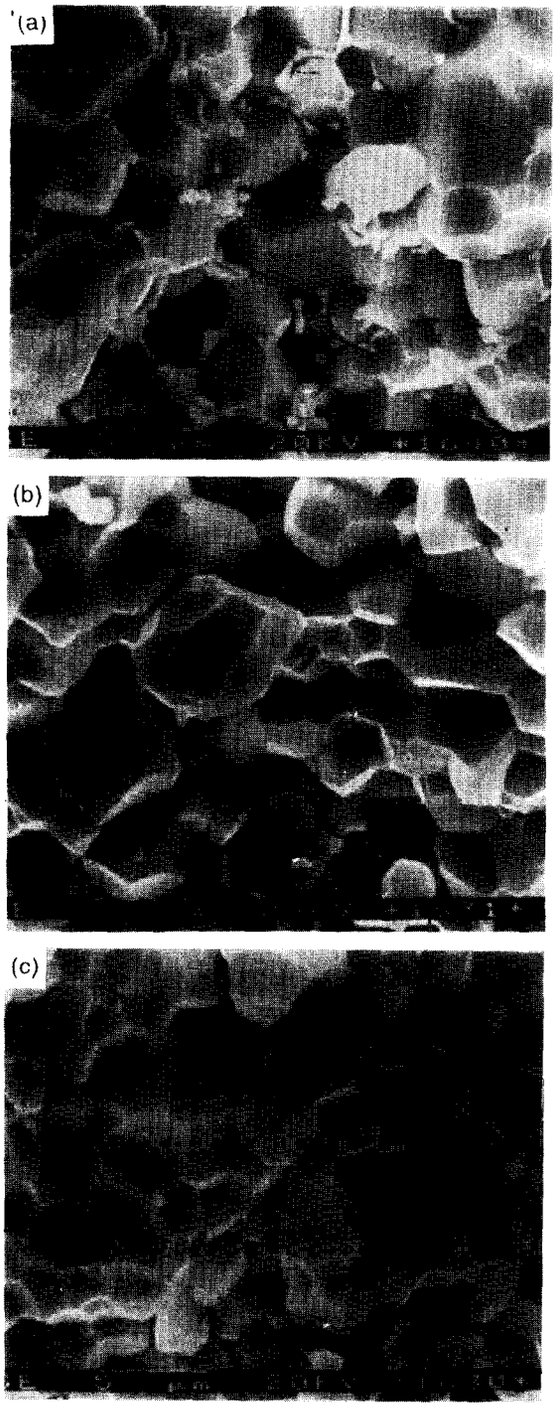

Fig. 7. Structures of aluminium nitride ceramics: (a) N1; (b) N2; (c) N3.

We decided to include in the article hot pressed aluminium oxide material for two reasons. The main reason is the minimization of stress factors affecting the mechanical characteristics, the majority of which is additives. The second reason is that we managed to obtain the material with very broad grain size distribution only via hot pressing (N2). Abnormal grain growth takes place during sintering, as well as during hot pressing. So if we are going to discuss the final stages of sintering, it is necessary to also take into consideration "over-sintered" material. Also it is necessary to mention that the mechanical characteristics of the surfaces of hot pressed material should differ from those of sintered material because of macro-stresses.

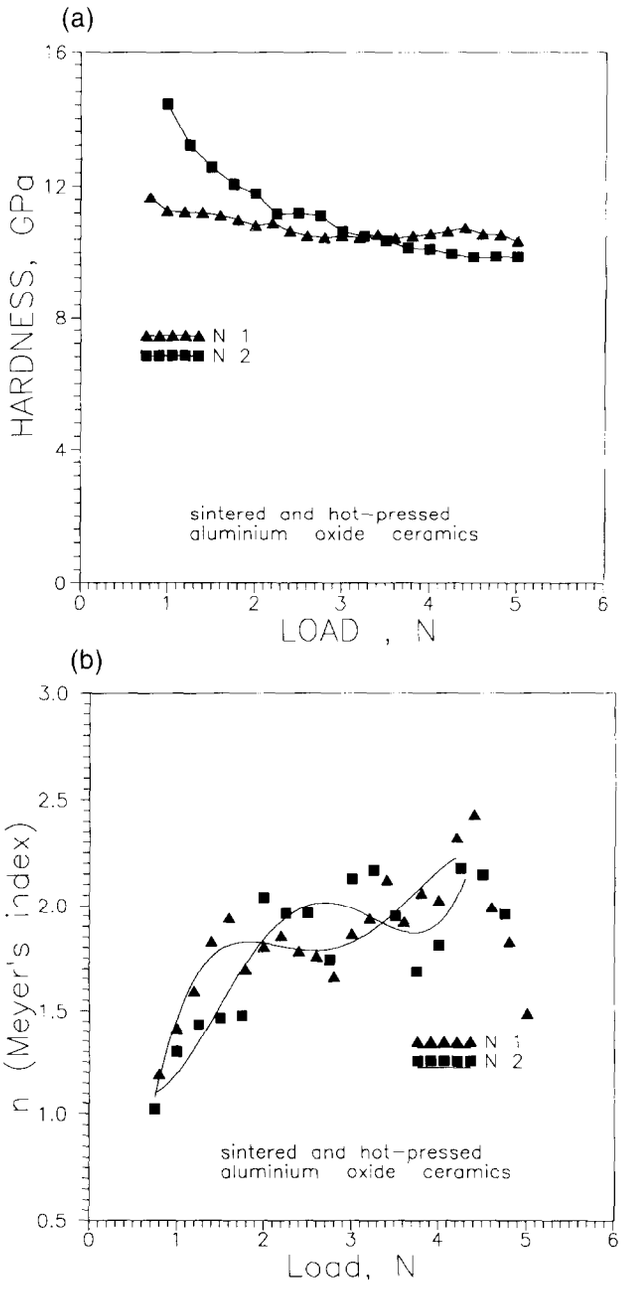

Fig. 8. Plots of (a) "hardness load" and (b) "Meyer's index n–load" for aluminium oxide ceramics.

The abnormal grain growth process is complex and originates from many possible causes, such as wide initial particle distribution, small amounts of liquid phase, inhomogeneous densification, presence of dopants and impurities, etc. In ceramics with inhomogeneous structure the thermal expansion anisotropy and or mismatch between large and small grains generates the thermal strains during cooling from the sintering temperature. The thermal strains sometimes cause grain-boundary cracking and sometimes remain as residual stresses at room temperature.

In sample N2 the secondary recrystallization caused by diffusion under the influence of stress gave rise to intense grain growth up to 20–30 μm. (Fig. 9). The grain size distribution is: 1–3 μm, 15%; 3–5 μm, 42%; 5–7 μm, 14%; 7–11 μm, 17%; 11–15 μm, 8%; 15–20 μm, 2%; >20 μm, the remainder. The bending strength is 400 ± 70 MPa, $K_{1c} = 2.7 \pm 0.96$ MPa·m$^{1/2}$ (determined by notch bend test).

The load dependence of hardness of aluminium oxide material N2 cannot add much about the structure of material, as well as dependence of Meyer's index n (Fig. 8). However, certain differences in mechanical characteristics of the surface between "normal" and "over-sintered" materials are realized in another way.

In real ceramic materials, the diagram "load–depth of indentation" is continuous and looks like that for steel (Fig. 4). Sometimes these diagrams for material with broad grain size distribution (N2) are continuous, and sometimes steps appear on "P–h" diagrams (Fig. 10(a)). The "step" is an intrusion of the indenter without additional application of load; this is realized in the case of cracks appearing on the grain boundary, cracking of the grain and chipping of part of the grain or subgrain. On Fig. 10(a) the steps take place at a load of 0.4 N (indentation N2), at a load of 2.8 N (indentation N1) and at a load of 4.8 N (indentation N2). This step on the "P–h" diagram results in rapid diminishing of hardness on the appropriate dependence "hardness–load" (Fig. 10(b)). If there is no step on the "P–h" diagram there are usually inflections, as shown on diagram N4. This also shows a change of "law" of intrusion of the indenter in micro-strained material.

Ma and Clarke[7] investigated the dependence of residual stresses on grain size in coarse-grained alumina with the help of piezo-spectroscopic measurements. A notable feature of their data is that

Fig. 9. Structure of hot pressed aluminium oxide material N2.

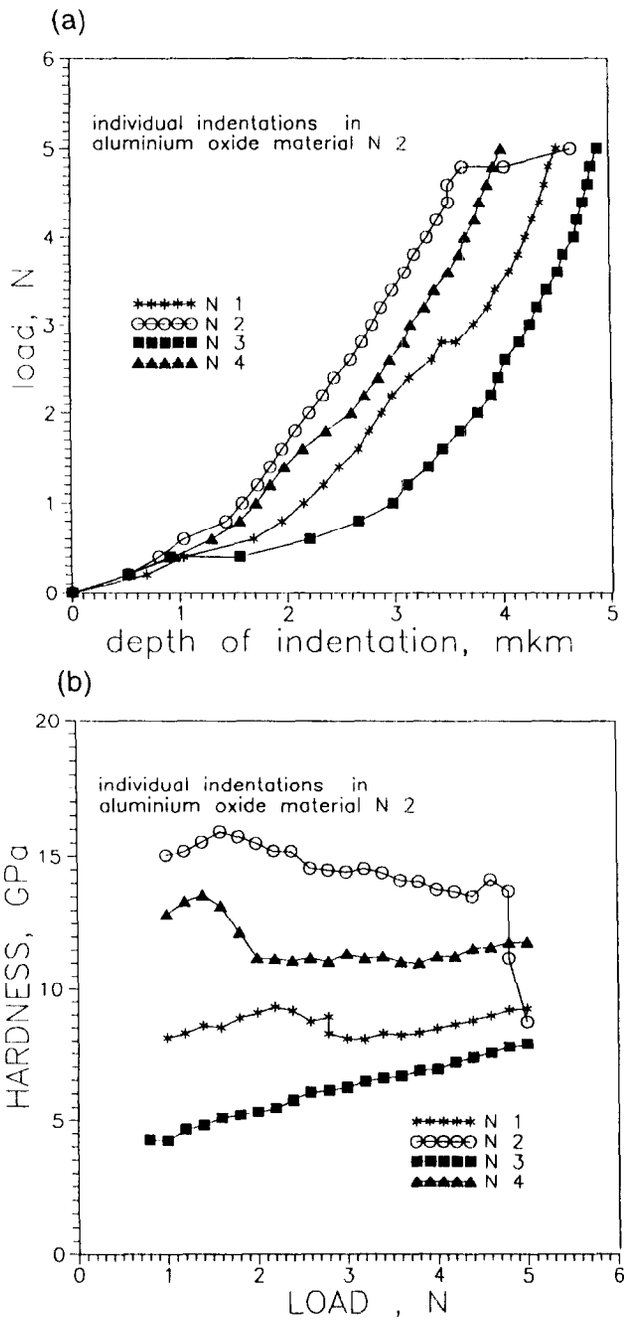

Fig. 10. Individual (non-averaged) plots of (a) "load–depth of indentation" and (b) "hardness–load" for aluminium oxide ceramics.

the observed variations in the average value of residual stress are considerably larger than the average value. The spatial variations in the average stress exist over millimetre distance and larger.

Our data shows that at a load of 1 N the deviations of hardness from the average value (that has a dimension of stress) in coarse-grained alumina reaches 19 GPa, that is 266%, and at 3 N reaches 12.7 GPa, that is 220%. Our experience shows, that such materials have poor polishing ability — grains or parts of grains of the polished material chip or pull out under the grains of the abrasive.

The coefficient of variation characterises the spread of values of microhardness, and deviations from the average value (eqn (2)). Abnormal grain growth and micro-strained structure gives a spread of values of microhardness 6–7 times greater than in the case of "normal material–SiAlON material" N3 or aluminium nitride material N3, and 20 times greater than in the case of steel (Fig. 3).

The coefficient of variation of values of microhardness is a comparative characteristic, but may be useful together with other characteristics of the surface.

3.5 General considerations

The final stage of sintering determines the characteristics of the material. Usually, the final stages of sintering are optimized via residual porosity and grain size and shape (these are believed to control mechanical characteristics) with the help of temperature and time of sintering.

The load dependence of hardness study can also be an instrument of optimization of the final stages of sintering. If load dependence of hardness reaches a plateau, we may suppose that the sintering process in that material had finished perfectly. Meyer's index at the plateau reaches a value of 2. All other variants (load dependence of hardness reaches a plateau with a slope or does not reach a plateau at all) signify that something is wrong with the structure of the sintered material. The sintering process in such a material may not be finished up to the end, resulting in small amounts of residual porosity, or in a failure to develop the strict crystallographic facets of grains of material. The other variant is the beginning of abnormal grain growth, that also gives a sloping load dependence of hardness.

However, the experience with hot pressed alumina shows that the material with broad grain size distribution can also demonstrate load dependence of hardness with a plateau (Fig. 8). In this case it is necessary to pay attention to individual indentation curves and to the coefficient of variation of values of microhardness. The coefficient of variation is a comparative characteristic and usually it shows violations of the structure of the material.

4 CONCLUSIONS

The following conclusions can be drawn from the work described above:

1. The load dependence of hardness study can be an instrument of optimization of the final stages of sintering. Load dependence of hardness of a perfect material reaches a plateau. Meyer's index n at the plateau reaches a value of 2.
2. Load dependence of hardness reaches a plateau with a slope or does not reach a plateau at all in material with an imperfect structure. The reasons may be small amount of residual porosity, absence of strict crystallographic facets of grains or non-uniform grain size distribution. Meyer's index would not reach a value of 2.
3. Large values of the coefficient of variation of microhardness (compared with a standard material) usually show a non-uniform grain size distribution. Micro-cracking and chipping of parts of grains results in steps and inflections on the individual indentation curves.

ACKNOWLEDGEMENT

The authors are grateful to Dr V. N. Skvortsov (Institute for Machine Science, Russian Academy of Science, Moscow) for support and discussions of results.

REFERENCES

1. EXNER, H. E., Sintering process. In *Sintering Key Papers*, ed. Sh. Somiya & Yu. Moriyoshi. Elsevier, London, New York, 1990, pp. 801, 157–184.
2. KINGERY, W. D., BOWEN, H. K. & UHLMANN, D. R., *Introduction to Ceramics*, 2nd edn (Wiley series on the Science and Technology of Materials). Wiley, New York, 1976, 1032 p.
3. YURKOV, A. L., JURAVLEVA, N. V. & LUKIN, E. S., Kinetic microhardness measurements of SiAlON based ceramics. *J. Mater. Sci.*, **29** (1994) 6551–6560.
4. ANTIS, G. R., CHANTIHUL, P., LAWN, B. R. & MARSHALL, D. B., A critical evaluation of indentation techniques for measuring fracture toughness: I. Direct crack measurements. *J. Am. Ceram. Soc.*, **64** (1981) 533–538.
5. BULYICHEV, S. I. & ALEKHIN, V. P., *Testing of Materials with Continuous Intrusion of Indenter* (in Russian). Moscow, Mashinostroyenie, Moscow, 1990, 224 p.

6. LI, H. & BRADT, R. C., The indentation load size effect and the measurement of hardness of vitreous silica. *J. Non-Cryst. Solids*, **146** (1992) 197–212.

7. MA, Q. & CLARKE, D. R., Piezospectroscopic determination of residual stresses in polycrystalline alumina. *J. Am. Ceram. Soc.*, 77(N2) (1994) 298–302.